Plasma Phys. Control. Fusion **50** (2008) 124025 (11pp) doi:10.1088/0741-3335/50/12/124025

The interaction of a flowing plasma with a dipole magnetic field: measurements and modelling of a diamagnetic cavity relevant to spacecraft protection

R Bamford[1], K J Gibson[2], A J Thornton[2], J Bradford[1], R Bingham[1,6], L Gargate[1,3], L O Silva[3], R A Fonseca[3], M Hapgood[1], C Norberg[4], T Todd[5] and R Stamper[1]

[1] Space Plasmas, Rutherford Appleton Laboratory, Chilton, Didcot, OX11 0QX, UK
[2] Department of Physics, University of York, Heslington, York, YO10 5DD, UK
[3] Centro de Física dos Plasmas, Inst Superior Técnico, 1049-001 Lisboa, Portugal
[4] Department of Space Physics, Umea University, Box 812, 981 28 Kiruna, Sweden
[5] EFDA-JET, Culham Science Centre, Abingdon, Oxfordshire, OX14 3DB, UK

Received 2 June 2008
Published 4 November 2008
Online at stacks.iop.org/PPCF/50/124025

Abstract

Here we describe a new experiment to test the shielding concept of a dipole-like magnetic field and plasma, surrounding a spacecraft forming a 'mini magnetosphere'. Initial laboratory experiments have been conducted to determine the effectiveness of a magnetized plasma barrier to be able to expel an impacting, low beta, supersonic flowing energetic plasma representing the solar wind. Optical and Langmuir probe data of the plasma density, the plasma flow velocity and the intensity of the dipole field clearly show the creation of a narrow transport barrier region and diamagnetic cavity virtually devoid of energetic plasma particles. This demonstrates the potential viability of being able to create a small 'hole' in a solar wind plasma, of the order of the ion Larmor orbit width, in which an inhabited spacecraft could reside in relative safety. The experimental results have been quantitatively compared with a 3D particle-in-cell 'hybrid' code simulation that uses kinetic ions and fluid electrons, showing good qualitative agreement and excellent quantitative agreement. Together the results demonstrate the pivotal role of particle kinetics in determining generic plasma transport barriers.

1. Introduction

A major issue for the future of manned space exploration is the potentially lethal damage to human tissue from exposure to radiation in space arising, for example, from the solar wind. The solar wind consists of a plasma characterized by low densities ($(0.1–2) \times 10^6\,\mathrm{m}^{-3}$),

[6] Also at: Physics Department, University of Strathclyde, Glasgow, G4 0NG, UK.

moderate temperatures (10–300 eV) and fast/supersonic (300–1000 km s^{-1}) directed flows; the actual solar wind output is highly variable on time scales of milliseconds upwards due to the localized and turbulent origins of the energetic plasma from the surface of the Sun. The solar magnetic field is carried with the out-flowing plasma and is of the order of 2–10 nT at the distance of the Earth's orbit. Of greatest concern from a manned spacecraft safety standpoint are the energetic (10–100 MeV) heavy solar wind particles of which ∼90% are protons, 9% are alphas, with electrons making up the majority of the remaining mass.

With the exception of the Apollo missions in the 1960s and early 1970s, manned space missions, including the International Space Station (ISS), have not ventured beyond low-Earth-orbit (LEO) at approximately 300 km altitude. This close to the Earth the atmosphere is still significantly dense (∼10^{11} cm^{-3}) to attenuate much of the particle flux from space. Above this height there is the additional protection created by the magnetosphere. This is the magnetized plasma structure created as a consequence of the Earth's magnetic dipole field as it extends out into the realms of space. Since the 1960s there has been interest in the viability of creating artificial magnetosphere structures to provide local protection of spacecraft instrumentation and astronauts [1, 2], but these and subsequent studies [3–5] were criticized as requiring impractically large power supply and coil assemblies to create the necessary field strengths [6]. However, these analyses were largely based on rather simplistic, essentially single particle approaches when evaluating the necessary magnitude of the protecting field rather than considering collective plasma effects that might be expected to dominate in such scenarios. Recent work [7] on 3D hybrid modelling of the plasma–dipole field interaction suggests that more modest field strengths may indeed be effective at creating diamagnetic-like cavities (regions in which energetic ionized particles are essentially absent) that have the potential for spacecraft shielding. These modelling studies have encouraged the development of laboratory analogues to the solar wind–spacecraft interaction system (for a recent review of laboratory experiments of relevance to space plasmas see [8]), similar to those used to explore the potential of using mini-magnetosphere structures as a means of aiding spacecraft propulsion [9].

In this paper we report on initial experiments in which a magnetized flowing plasma beam is incident upon a dipole magnetic field structure, seeking to simulate in the laboratory the effect of such field structures on incident solar wind particles. In the next section we outline the experimental apparatus and diagnostics used in this work. In section 3 we report on spatially resolved measurements of the principal plasma parameters and compare these results with simple analytical models as well as predictions from the dHybrid kinetic simulation. Finally, in section 4 we summarize the results of this study and outline future needs for further experimental investigations of spacecraft protection systems.

2. Experimental apparatus

The experimental studies were carried out on a linear plasma confinement device LinX, a modified version of the ULS device [10] previously used to study plasma–neutral interactions of relevance to tokamak divertors [11, 12]. The plasma in this system consists of a supersonic plasma beam (Mach number>3) with peak densities and temperatures in the range 10^{17}–10^{19} and 5–7 eV, respectively. Figure 1 shows a schematic diagram of the experimental set-up showing the principal components of the device as configured for these studies, including the dipole magnetic field source and the location of the main diagnostics.

The LinX vacuum vessel, constructed of non-magnetic stainless steel, is cylindrical with length of 1.5 m and diameter of 24 cm and is pumped by diffusion pumps that are isolated by gate valves and located at each end of the device. The solenoidal field coils, connected in

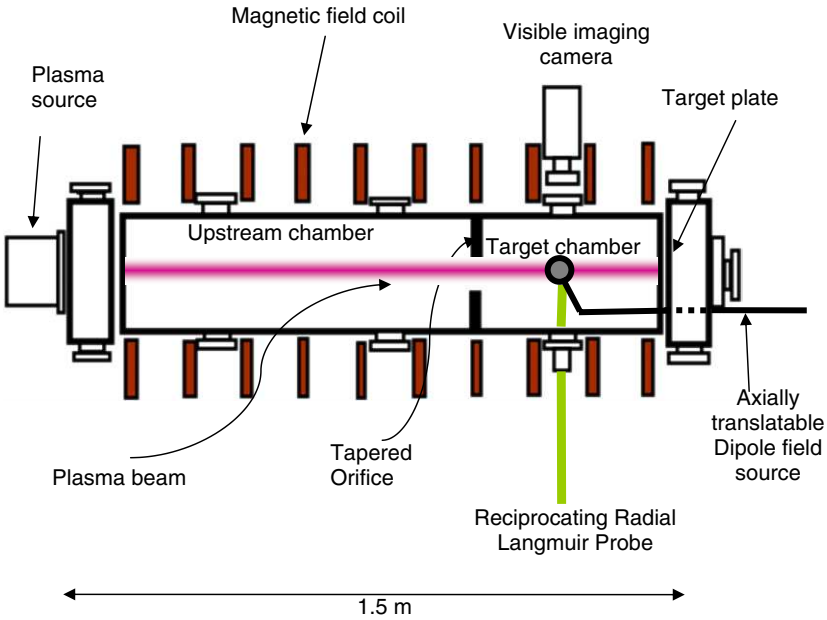

Figure 1. Overview of the experimental arrangement using the LinX linear plasma device indicating the geometry of the device and the location of the principle plasma diagnostics used in these studies.

series with a single return conductor to cancel the error field due to the connecting straps, have inside diameters of 28 cm and are placed 14.5 cm apart: the maximum field at the centre of the machine for the work reported here is approximately 0.07 T. For these studies, this linear field represents the analogue of the interplanetary magnetic field. The vacuum vessel is divided by a diaphragm containing a small orifice (14 mm diameter) to separate off the 'target chamber' in which an increased gas pressure (in the range 0.5–3 mTorr, corresponding to neutral densities of approximately 1.5×10^{19}–1×10^{20} m^{-3}) can be maintained, enhancing visible light emission and enabling better use of fast imaging diagnostics. The plasma source [13] is a development of a modified 'duoplasmatron' source and the plasma output contains a mixture of ions H^+, H_2^+ and H_3^+; for the work reported here, the proportions are roughly 90%, 5% and 5%.

Two dipole field sources were used in these studies. The first, a permanent, cylindrical magnet (with field strength at the pole of approximately 0.2 T), was mounted on a probe manipulator which allowed it to be moved to various axial positions along the target chamber. The second magnet source was a pulsed system formed from a 10 turn solenoid with a maximum current of 3.5 kA/turn. Again this source produces a dipole field structure but at significantly stronger field strengths (over 2 T at the pole). This dipole source allowed the dynamics of the interaction to be investigated using a high speed visible camera and a fast Langmuir probe acquisition system.

The diagnostics used in these studies are primarily based on electrical probes and fast imaging cameras. Langmuir probes, mounted on reciprocating probe holders so as to minimize the deleterious effects of probe heating by the plasma beam, allow the acquisition of radial profiles (with a spatial resolution of 1 mm) of electron density and temperature at various positions within the target and upstream chambers. The data acquisition system (Hiden Analytical) allows a full profile to be obtained in a few tens of seconds, the time over

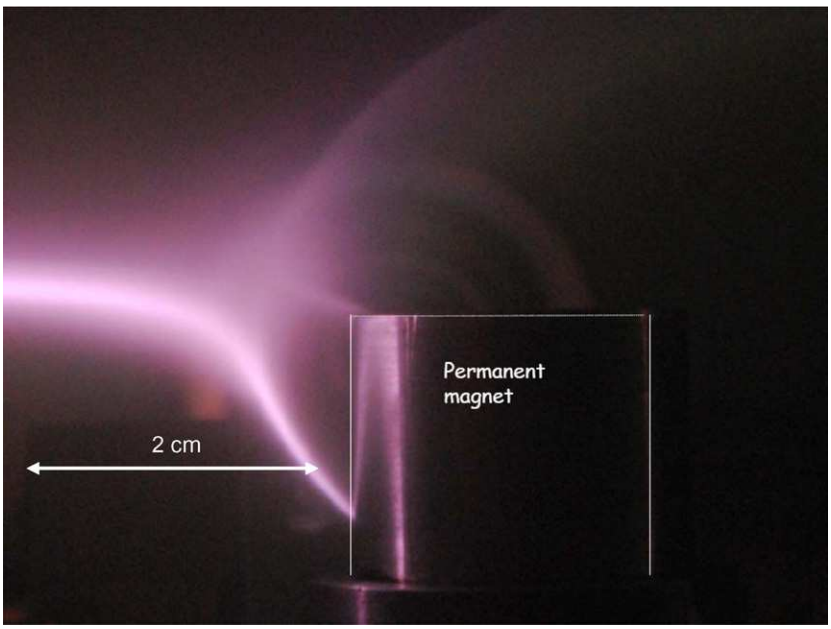

Figure 2. Visible light image of the plasma beam on LinX incident on a dipole magnetic field. The beam is incident from the left-hand side of the image at an impact parameter approximately 2 mm above the upper face (pole) of the dipole magnet and it is apparent that the beam is deflected around the dipole field structure, forming a thin annular sheet.

which any variation in plasma source output is minimized. By a combination of the radial scanning of the probe system and moving the axial position of the dipole field source, it is possible to obtain 2D maps of plasma parameters around the plasma–dipole field interaction region.

For imaging studies a high speed visible camera (Photron APX-RS) allows image acquisition at frame rates of up to 250 000 frames s^{-1}: in practice, the maximum frame rate was limited by the available light to 50 000 fps. Figure 2 shows an example of a visible light image (in this case the integration time is approximately 1 ms) of the plasma beam interacting with the permanent dipole magnet. The visible light emission (predominantly hydrogen Balmer series emission which originates from interaction of the plasma with the background neutral gas) corresponds to regions of higher plasma density, and it is apparent that the plasma beam is deflected in an apparently stable narrow layer around the magnet casing.

3. Results and modelling

3.1. Upstream plasma beam characteristics

Initial results were obtained for the interaction of the plasma beam with the static dipole field. The 'upstream' (i.e. in a region sufficiently distant from the region in which the dipole field dominates) electron density and temperature for this case were $3 \times 10^{17}\,m^{-3}$ and 3 eV, respectively. In the absence of the downstream dipole field structure it would be expected that this plasma would propagate along the solenoidal confining field until it encountered the end target plate of the gas target chamber. Previous studies at low target chamber gas pressures

similar to those used in these studies have indicated that any reductions in the peak density or temperature occur over characteristic axial scale lengths >1 m with the beam width (FWHM) remaining constant along the whole length of the target chamber [10]. This is consistent with the expected collisional scale lengths for these plasmas: the ion–ion mean free path is of the order of 10 m and the typical ion–neutral mean free path is approximately 25 cm, an order of magnitude greater than the ion Larmor radius.

Typically the plasmas produced in LinX are supersonic and in the absence of any direct ion energy measurements, for these studies there are indications of such directed flows from the relative magnitudes of the floating and plasma potentials. Defining the sheath coefficient α in the usual way in terms of the floating potential (φ_f) and the plasma potential φ_p such that $\varphi_p = \varphi_f + \alpha T_e$, an expression due to Lipschultz *et al* [14] for a hydrogen plasma with an isotropic velocity distribution, subsonic ion flow and no secondary emission suggests a value for α of 3.3. Using the direct measurement of the upstream floating potential and evaluating the plasma potential using the second derivative of the Langmuir probe characteristic [15], we obtain $\alpha = 1.7$, considerably less than that expected for an isotropic plasma. Supersonic ion flow will tend to reduce the value of α and a more detailed analysis [10, 13, 16, 17] suggests a full expression for α:

$$\alpha = -\frac{1}{2}\ln(2\pi\mu\Psi^2 M^2(1+\gamma_s^2)),$$

where $\mu = m_e/m_i$ is the mass ratio, γ_s is the secondary emission coefficient, Ψ is the ratio of the probe collection areas for ions and electrons and M is the Mach number at the sheath boundary (i.e. valid for $M \geqslant 1$). Assuming equal probe collections areas and that the secondary emission coefficient is zero, a value of $\alpha = 1.7$ is consistent with these plasmas having $M \sim 3$.

3.2. Interaction with static dipole field

A series of Langmuir probe scans have allowed the spatial structure of the plasma to be determined in a plane 2 mm above the pole of the static dipole field source. Figure 3 shows contour plots of density and floating potential in this plane. The results generally support the impression given by visible imaging in figure 2, indicating that the supersonic flowing plasma is deflected around the dipole field source, forming a thin, approximately annular sheet of plasma. The thickness of this sheet is of the order of 3–4 mm, of the order of 10 times less than the ion Larmor radius of the energetic, flowing ions. The measurement of the characteristic scale length of the deflected sheet provides an indication of the role of collective effects in the shielding process.

Figure 4 shows details of the profiles for axial positions of $x = -60$ mm, $x = 20$ mm and $x = 50$ mm, where $x = 0$ corresponds to the axial position of the pole of the dipole source; negative values relate to upstream positions and positive values relate to downstream positions. These profiles confirm the spatial scale of the deflected plasma layer, clearly showing that the impinging plasma beam is deflected off axis. A careful examination of these profiles reveals the presence of an electrostatic 'potential well' which confines the ions; the depth of this potential well (approximately 2 V) is consistent with the expected transverse ion energy [10].

Figure 5 shows the axial variation of the plasma density and floating potential along the axis of the beam. Once again, the pole of the dipole source is located at $x = 0$ and the shaded region corresponds to the magnet casing size. It can be seen that the reduction in plasma density on axis corresponds to a region in which a significant electrostatic potential gradient exists. The step in potential (of the order of 5–10 V) is consistent with the expected energy of the impinging ions, again providing evidence for the role of ambipolar electric fields in forming a transport barrier around the dipole field region. Also of interest in figure 5 is the region directly

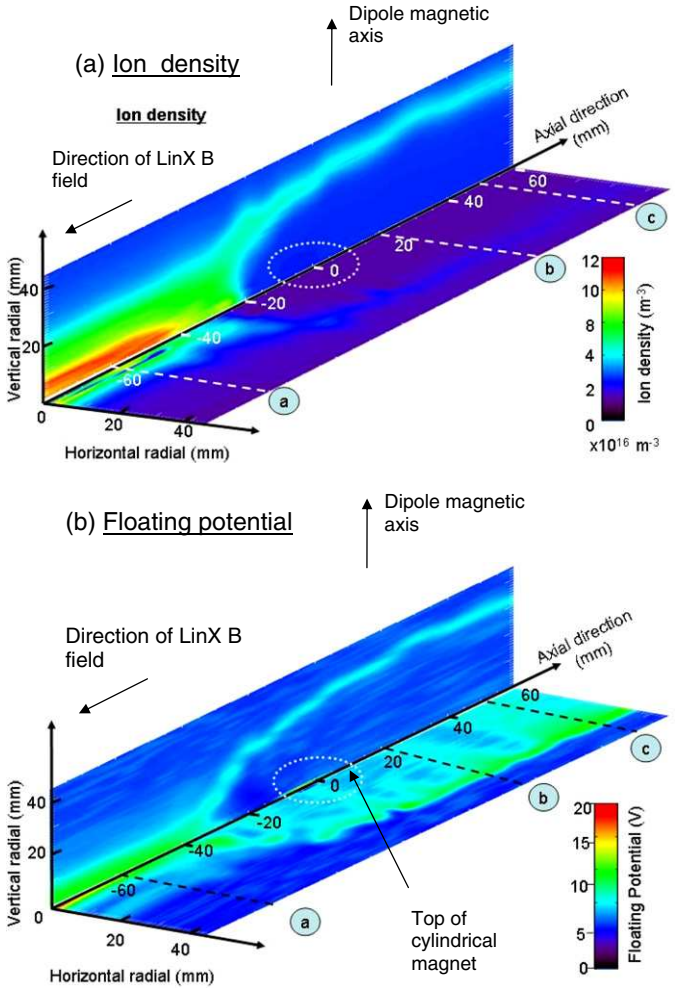

Figure 3. The 2D profiles of (*a*) plasma density and (*b*) floating potential obtained using a radial scanning Langmuir probe. The position of the dipole magnet (indicated by the dotted line) is moved relative to the probe position to provide axially resolved measurements. The dotted lines, labelled a, b and c, correspond to the positions of the radial profiles shown in figure 4.

above the pole of the dipole source where there are indications of a local potential structure: this would appear to correspond to the area of enhanced emission (figure 2) that connects the region where there is expected to be a localized field null (analogous to the polar cusp of a magnetosphere) to the pole of the dipole field source and future work will seek to characterize this feature in more details.

As outlined in the previous section, subject to certain assumptions, the sheath coefficient, α, can be used to indicate the Mach number of the plasma beam and figure 6 shows the variation of α as a function of the axial position along the beam centreline. The data are consistent with the beam being slowed from $M > 3$ to subsonic flows as it enters the region corresponding to the potential gradient in figure 5.

Initial modelling of the plasma beam–dipole field interaction has been undertaken [7]. Since the typical time and the length scales in the mini-magnetospheres in the laboratory are

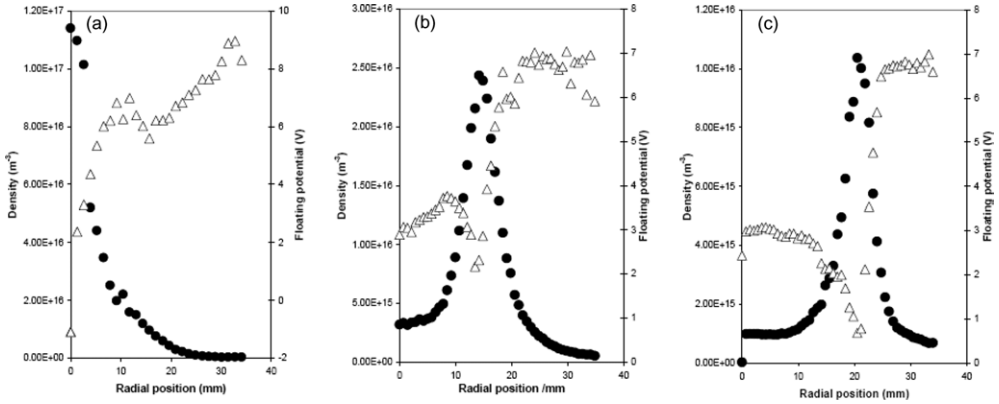

Figure 4. Details of Langmuir probe profiles of density (closed circles) and floating potential (open triangles) at (*a*) −60 mm, (*b*) +20 mm and (*c*) +50 mm axial positions (where 0 mm corresponds to the pole of the dipole field source). The profiles indicate that the deflected layer of plasma occupies a narrow region of the order of 4 mm and also reveal the presence of a local potential well that confines the ions perpendicular to the local magnetic field.

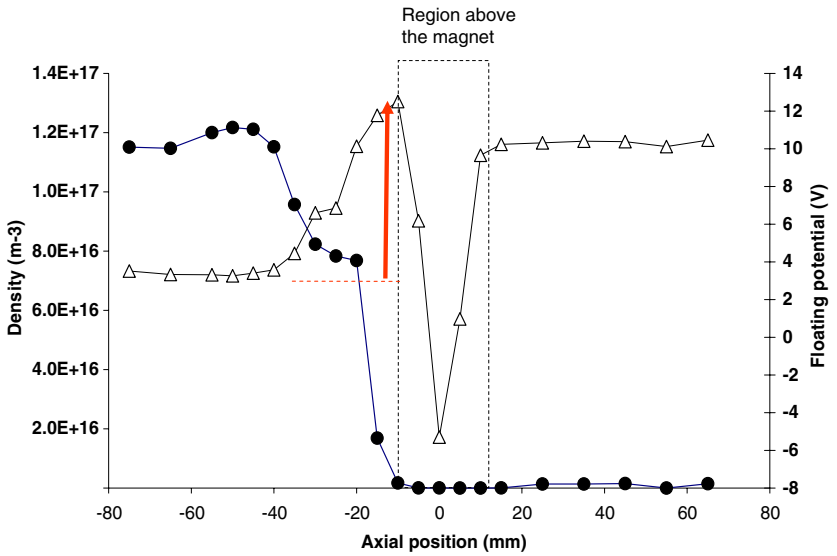

Figure 5. Axial profile of density (closed circles) and potential (open triangles) along the centre of the beam, showing the presence of an electrostatic barrier as the beam impacts the dipole field region. The shaded region corresponds to the physical extent of the dipole source casing; the potential structure around this casing is believed to be related to plasma inflows at the polar cusp.

large, three-dimensional kinetic particle-in-cell simulations, where both ions and electrons are treated kinetically, are not feasible. We resort instead to hybrid simulations, using the code dHybrid [18], a hybrid code with kinetic ions and fluid electrons. In the hybrid approximation [19], the displacement current in Ampere's law is neglected, quasi-neutrality is assumed and moments of the Vlasov equation for the electrons are calculated in order to obtain the generalized Ohm's law, which yields the electric field. Using the experimentally determined

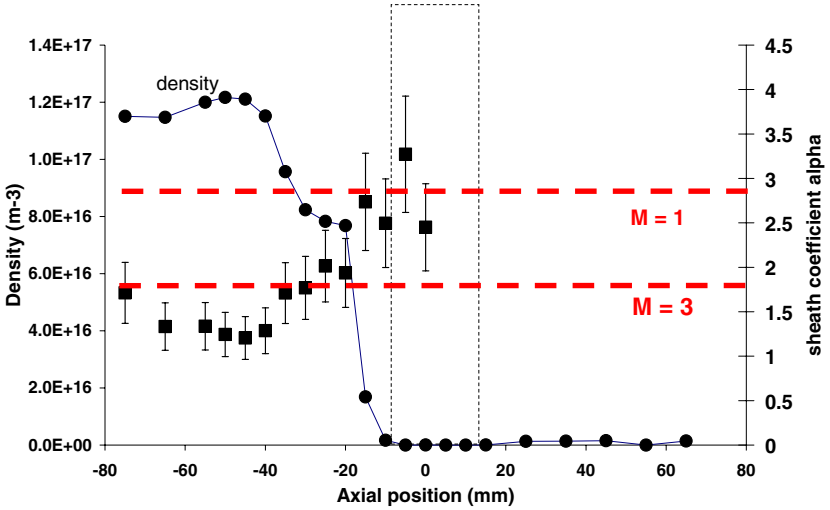

Figure 6. Plot of the sheath coefficient, α (squares) and the ion density (circles) as a function of the axial distance along the centre of the plasma beam ($x = 0$ corresponds to the centre of the pole of the dipole field source). The value of α can be used to infer the Mach number of the plasma beam (values for $M = 3$ and $M = 1$ are shown assuming equal ion and electron probe collection areas and zero secondary emission coefficient), indicating the beam slowing as it approaches the potential barrier shown in figure 5.

upstream plasma parameters, dHybrid has been used to simulate the LinX experiments. Figure 7 shows a 2D profile of plasma density, with darker colours indicating regions of lower plasma density. Comparing with the measured profiles in figure 2, it is apparent that the code is successful in reproducing the basic experimental results, with a clear indication of a diamagnetic cavity being formed around the dipole field region. The characteristic scale lengths of density around the transport barrier region are comparable to those obtained experimentally and the 'stand-off' distance (the position in front of the dipole field source at which the incoming flowing plasma is deflected) is also well matched (within 7%) to experiment.

3.3. Interaction with pulsed dipole field

Finally, we briefly report on ongoing experiments using a pulsed dipole field source. This source, outlined in section 2, operates with current pulses of up to 3.5 kA of approximately 5–10 ms duration and with characteristic rise times of approximately 100 μs. The field at the pole corresponding to these currents can approach 2 T, approximately an order of magnitude greater than in the static field experiments. In these initial experiments a Langmuir probe, biased well into the ion saturation region of the I–V characteristic, was positioned 2 mm above the front edge of the solenoid casing. The current drawn to the probe (by convention this current has a negative sign) is sampled at 100 kHz, well within the bandwidth of the probe amplifier system. Figure 8 shows a time history of the ion saturation current overlaid with the field solenoid current. It is apparent that the ion saturation current is reduced by more than two orders of magnitude, consistent with measurements using the static dipole system. In particular, the current is approximately zero between 1 and 3 ms, corresponding to a period when the diamagnetic cavity is fully established. While much further work is necessary to analyse this configuration, it is striking that the apparent field required to form this cavity appears to be much greater than that needed to sustain it. This is apparent from the

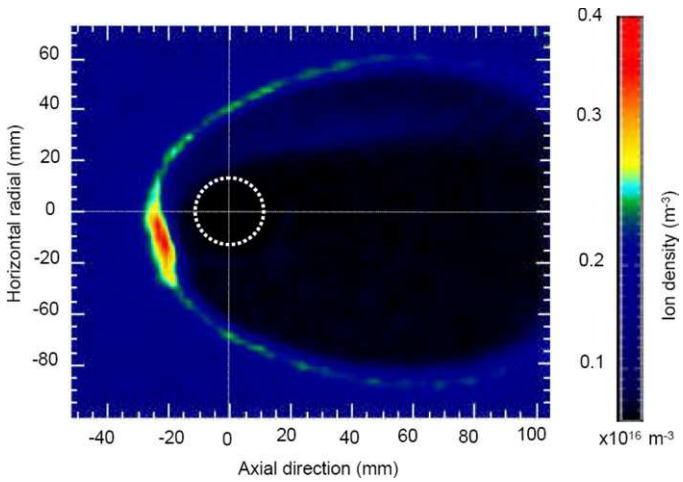

Figure 7. dHybrid simulation results showing the appearance of diamagnetic-like cavity in good agreement with the structures identified experimentally in figure 3. In particular, the characteristic scale lengths of the transport barrier (apparent from the brighter regions of higher density) are well matched with experiment, being considerably less than the scale length of the ion Larmor radius.

large hysteresis effect in solenoid current/ion saturation current space. Whilst the origin of this effect is uncertain at present, it may have important practical implications for the power requirements for possible future spacecraft protection systems.

4. Summary and conclusions

Initial laboratory experiments in which a fast flowing magnetized hydrogenic plasma impacts upon a dipole field structure have been undertaken in order to help evaluate their potential for spacecraft protection systems. Visible light imaging of the system indicates that the plasma beam is deflected into a thin annular shell, the interior of which appears to be devoid of plasma. Measurements with Langmuir probes have confirmed the overall spatial structure identified by imaging and have indicated that the gradient scale lengths at the boundary of this diamagnetic cavity are considerably less than the ion Larmor radii. Spatial measurements of the floating potential within the plasma indicate that the ions in this system are essentially confined electrostatically.

Initial hybrid modelling of the system with the dHybrid code shows very good agreement with the experimental results, reproducing well the measured 'stand-off' distance and the overall spatial scale of the diamagnetic cavity. In addition the scale length of the transport barrier region is consistent with experimental results, being considerably shorter than the ion Larmor radius for the energetic ions. Together the experimental and modelling results demonstrate the pivotal role of particle kinetics in determining the plasma transport barriers expected in artificial mini-magnetospheres.

Future work will seek to extend these results to enable a proper scaling of the scale of the diamagnetic cavity with field strength and also to characterize in more detail the transport barrier at the boundary of the cavity, in particular, to study the stability and micro-turbulence associated with this structure. In addition, although the 2D maps of density and potential have been useful in characterizing the mini-magnetosphere, some regions (e.g.

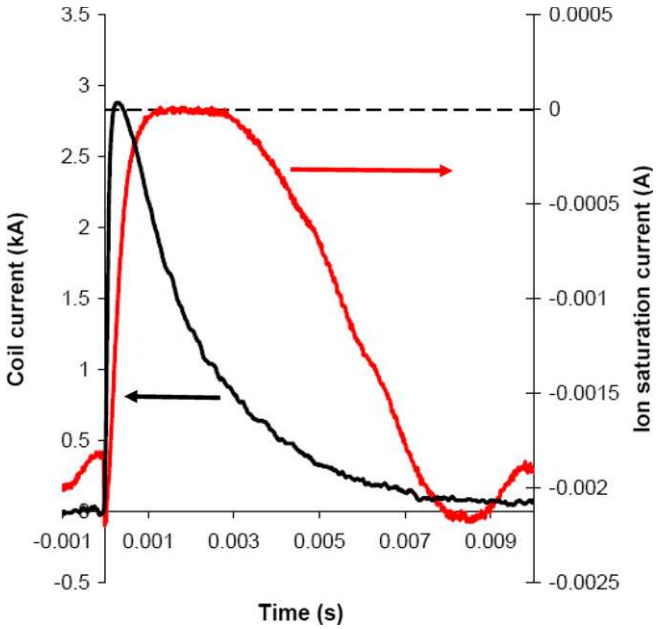

Figure 8. Temporal history of pulsed solenoid current (black) and ion saturation current (red), measured 2 mm above the front face of the solenoid casing. The shielding effect of the pulsed field is apparent from the reduction in ion saturation current to very low values (1–3 ms): also note the apparent hysteresis effect in the current required to establish and maintain this shielding.

around the polar cusps) have structures that will need more detailed three-dimensional spatial measurements.

Finally, we note that the LinX experiment, and other similar devices, offers an ideal platform to study a range of fundamental plasma physics phenomena that are of relevance to astrophysical contexts. With appropriately scaled dimensionless plasma parameters such machines have an important role to play in elucidating the fundamental physics of future mini-magnetosphere systems and in validating advanced kinetic plasma simulations.

Acknowledgments

The authors gratefully acknowledge the financial support of the United Kingdom Science and Technology Facilities Council.

References

[1] Levy R H and French F W 1968 *J. Spacecr.* **5** 570
[2] French F W 1970 *J. Spacecr.* **7** 794
[3] Cocks F H and Brit J 1991 *Interplanet. Soc.* **44** 99
[4] Hilinski E J and Cocks F H 1992 *J. Spacecr.* **31** 342
[5] Lanzerotti L 2004 *Space Weather* **2** S10001
[6] Parker E N 2006 *Sci. Am.* **294** 40
[7] Gargate L *et al* 2008 *Plasma Phys. Control. Fusion* **50** 074017
[8] Koepke M E 2008 *Rev. Geophys.* **46** RG3001
[9] Winglee R M, Slough J, Ziemba T and Goodson A 2000 *J. Geophys. Res.* **105** 21067–77

[10] Rusbridge M G *et al* 2000 *Plasma. Phys. Control. Fusion* **42** 579
[11] Browning P K *et al* 2005 *J. Nucl. Mater.* **337** 232
[12] Mihaljcic B, Browning P K and Gibson K J *Phys. Plasmas* **14** 013501
[13] Bradley J W *et al* 1995 *Plasma Sources Sci. Technol.* **4** 516
[14] Lipshultz B, Hutchinson I H, LaBombard B and Wan A 1986 *J. Vac. Sci. Technol.* **4** 1810
[15] Amemiya H *Japan. J. Appl. Phys.* **25** 595
[16] Qaosim H 1996 *PhD Thesis* UMIST, Manchester, UK
[17] Bradley J W *et al* 1992 *J. Phys. D: Appl. Phys.* **25** 1443
[18] Gargate L, Bingham R, Fonseca R A and Silva L O 2007 *Comput. Phys. Commun.* **176** 419
[19] Lipatov A S 2002 *The Hybrid Multiscale Simulation Technology* (Berlin: Springer)